Bias Estimation and Calibration of a Pair of Laser Range Sensors ⋆

Srećko Jurić-Kavelj * **Ivan Petrović** *

* *University of Zagreb, Faculty of Electrical Engineering and Computing, Zagreb, Croatia (e-mail: {srecko.juric-kavelj, ivan.petrovic}@ fer.hr).*

Abstract: Laser range sensors (LRS) are ubiquitous in mobile robotics. They are usually modeled as having statistical error only, despite some having systematic error (bias) documented. This paper deals with bias estimation for laser range sensors in order to produce better calibration for two LRS. Assuming both LRS sense in the same plane, we propose an algorithm to estimate position and orientation of the second laser in the coordinate frame of the first laser, or vice versa. In order to truly have corresponding points in two LRS scans, we propose a calibration target. We use cylindrical objects of known radius, placed in the field of view of both LRS, perpendicularly to the sensing plane. Centers of circles that result from the intersection of the sensing plane and cylindrical objects then become corresponding points. Our algorithm first estimates cylinder centers, together with their respective uncertainties, and then using those results produces Euclidean transform estimate, together with it's respective uncertainty. The results of this algorithm can be used to gather very precise ground truth for people tracking applications with LRS. In case of occlusions, one has obvious benefits from two or more different viewpoints.

Keywords: Mobile robots and vehicles, Modeling and identification.

1. INTRODUCTION

People detection and tracking is recognized as one of the key technologies in the field of mobile robotics. A large number of approaches to laser range sensors (LRS) people tracking exist, e.g. Topp and Christensen (2005); Kluge et al. (2001); Fod et al. (2002); Schulz et al. (2003) to name a few. All of these approaches have their strengths and weaknesses, but they are hard to compare directly. Until Bernardin and Stiefelhagen (2008) proposed two metrics to evaluate multiple objects tracking algorithm performance (collectively named CLEAR MOT), there was no *standard* metric a researcher could report in order to compare his algorithm with other approaches. Yet, even most recent works like Luber et al. (2011) which do report one CLEAR MOT metric, lack the ground truth for the tracked objects in the data, therefore reporting only one of the two metrics. Luber et al. (2011) report multiple objects tracking accuracy (MOTA) which depends on number of mis-detections, false positives and mismatches of tracked objects. MOTA essentially evaluates the first half of the multiple objects tracking algorithm pipeline, i.e. detection and data association. The second CLEAR MOT metric, moving objects tracking precision (MOTP) is the total error in estimated position for matched object-hypothesis pairs over all frames, averaged by the total number of matches made. It shows the ability of the MOT algorithm to estimate precise object positions, independent of its skill at recognizing object configurations, keeping consistent trajectories, and so forth. MOTP essentially evaluates the second half of the MOT algorithm pipeline.

Motivated to obtain ground truth data with ubiquitous and very precise laser range sensors, we investigate automatic calibration of a pair of such sensors. In case of occlusions, one has obvious benefits from two or more different viewpoints. Assuming both lasers sense in the same plane, we propose an algorithm which finds Euclidean transform that represents the position and orientation of one laser in the coordinate frame of the other, similarly as in Sasaki and Hashimoto (2011). The algorithm also calculates uncertainties of the position and orientation estimates.

In the field of computer vision, algorithms for solving more general problems than this exist. E.g., 2D homography estimation, but it assumes known point correspondences in two views. In computer vision, corresponding points are obtained automatically by using a calibration pattern. With laser range sensors there are generally no corresponding raw measurements in two views, even though some algorithms in this field, e.g. the iterative closest point algorithm, make this assumption.

Therefore, we needed to devise a calibration object for lasers. Considering view invariance, we settle for cylinders perpendicular to the laser sensing plane, so that their intersection results in a circle. Our calibration setup is shown in Fig. 1. Centers of such circles can be used as corresponding points between two views. In contrast to our approach, Sasaki and Hashimoto (2011) use a mobile

⋆ This work has been supported by the Ministry of Science, Education and Sports of the Republic of Croatia under grant No. 036–0363078–3018. and by the EC's Seventh Framework Programme under grant No. 285939 (ACROSS).

Fig. 1. Experimental setup of two laser range sensors calibration

robot to generate corresponding points. They used Pioneer mobile robots, which are fairly circular, but they stipulated that the robot's center was at distance $d = 15$ cm in the direction of scanning from the center of the cluster of points belonging to the robot. This is a very rough approximation, and the authors acknowledge that for more accurate results they should use a model of the object.

This paper is organized as follows. Section 2 discuses the Euclidean transform estimation algorithm and is divided into subsections discussing individual aspects. Section 3 evaluates proposed algorithm on real world data obtained with SICK LMS 200 and 291 units. Section 4 concludes the paper.

2. ESTIMATION OF 2D EUCLIDEAN TRANSFORM BETWEEN TWO LASER RANGE SENSORS

2.1 Estimating circle from laser range data

Laser range readings are usually modeled as independent Gaussian random variables with true range as mean and known standard deviation, equal for all readings. In order to estimate the circle in maximum likelihood sense from this data, one should minimize the sum of squared distances from measured range and the intersection of the same laser beam with the estimated circle.

Given a circle C and a set of laser beams sensing it, we define observed variables $\Delta r_i = r_i^C - r_i$, where r_i^C is the range of the i-th laser beam to it's intersection with the circle C and r_i is the measured range by the laser. Assuming observations $\Delta r_i \sim \mathcal{N}(0, \sigma_r^2)$ are independent and identically distributed, we can define circle likelihood function given all observations

$$\mathcal{L}(C|r_1, r_2, \ldots, r_n) = \prod_{i=1}^{n} f(\Delta r_i; 0, \sigma_r^2)\,, \tag{1}$$

where $f(\Delta r_i; 0, \sigma_r^2)$ is the normal probability density function.

The circle estimate in maximum likelihood sense is

$$\hat{C}_{mle} = \arg\max_{C \in \mathbb{C}} \mathcal{L}(C|r_1, r_2, \ldots, r_n)\,. \tag{2}$$

Maximizing likelihood is the same as maximizing log-likelihood, due to monotonicity of the log function. Since observation pdfs are normal

$$f(\Delta r_i; 0, \sigma_r^2) = \frac{1}{\sqrt{2\pi\sigma_r^2}} e^{-\frac{\Delta r_i^2}{2\sigma_r^2}}\,, \tag{3}$$

it makes sense to work with log-likelihood. Our likelihood maximization problem becomes

$$\begin{aligned} \hat{C}_{mle} &= \arg\max_{C \in \mathbb{C}} \ln \mathcal{L}(C|r_1, r_2, \ldots, r_n) \\ &= \arg\max_{C \in \mathbb{C}} \left(-\frac{1}{2\sigma_r^2} \sum_{i=1}^{n} \Delta r_i^2 + \text{const.} \right)\,, \end{aligned} \tag{4}$$

or more condense

$$\hat{C}_{mle} = \arg\min_{C \in \mathbb{C}} \sum_{i=1}^{n} \Delta r_i^2\,. \tag{5}$$

The problem of estimating circle from laser range data becomes a nonlinear least-squares problem.

2.2 Finding covariance matrix of the estimated circle parameters

Since we cannot give a closed form solution for the circle estimate, we will also need to propagate the covariance matrix backwards, as described in Hartley and Zisserman (2004).

Consider a differentiable mapping f from a *parameter space*, $\mathbb{R}^M$ to a *measurement space* $\mathbb{R}^N$, and let a Gaussian probability distribution be defined on $\mathbb{R}^N$ with covariance matrix Σ. Let S_M be the image of the mapping f. We assume that $M < N$ and that S_M has the same dimension M as the parameter space $\mathbb{R}^M$. Thus we are not considering the over-parametrized case at present. A vector $\mathbf{p} \in \mathbb{R}^M$ represents a parametrization of the point $f(\mathbf{p})$ on S_M. Finding the point on S_M closest in Mahalanobis distance to a given point $\mathbf{x} \in \mathbb{R}^N$ defines a map from $\mathbb{R}^N$ to the surface S_M. We call this mapping $\eta : \mathbb{R}^N \to S_M$. Now, f is by assumption invertible on the surface S_M, and we define $f^{-1} : S_M \to \mathbb{R}^M$ to be the inverse function.

By composing the map $\eta : \mathbb{R}^N \to S_M$ and $f^{-1} : S_M \to \mathbb{R}^M$ we have a mapping $f^{-1} \circ \eta : \mathbb{R}^N \to \mathbb{R}^M$. This mapping assigns to a measurement vector $\mathbf{x}$, the set of parameters $\hat{\mathbf{p}}$ corresponding to the ML estimate $\hat{\mathbf{x}}$. In principle we may propagate the covariance of the probability distribution in the measurement space $\mathbb{R}^N$ to compute a covariance matrix for the set of parameters $\mathbf{p}$ corresponding to ML estimate.

If f is affine, we may write $f(\mathbf{p}) = f(\bar{\mathbf{p}}) + J(\mathbf{p} - \bar{\mathbf{p}})$, where $f(\mathbf{p}) = \mathbf{x}$ is the mean of the probability distribution on $\mathbb{R}^N$. Since we are assuming that the surface $S_M = f(\mathbb{R}^M)$ has dimension M, the rank of J is equal to its column dimension. Given a measurement vector $\mathbf{x}$, the ML estimate $\hat{\mathbf{x}}$ minimizes $\|\mathbf{x} - \hat{\mathbf{x}}\|_\Sigma = \|\mathbf{x} - f(\hat{\mathbf{p}})\|_\Sigma$. Thus, we seek $\hat{\mathbf{p}}$ to minimize this latter quantity. However,

$$\|\mathbf{x} - f(\hat{\mathbf{p}})\|_\Sigma = \|(\mathbf{x} - \bar{\mathbf{x}}) - J(\hat{\mathbf{p}} - \bar{\mathbf{p}})\|_\Sigma \tag{6}$$

and this weighted least-squares problem is minimized when

$$\hat{\mathbf{p}} - \bar{\mathbf{p}} = (J^{\mathrm{T}}\Sigma^{-1}J)^{-1}J^{\mathrm{T}}\Sigma^{-1}(\mathbf{x} - \bar{\mathbf{x}})\,. \tag{7}$$

Writing $\bar{\mathbf{p}} = f^{-1}(\bar{\mathbf{x}})$ and $\hat{\mathbf{p}} = f^{-1}(\hat{\mathbf{x}})$, we see that

$$\begin{aligned} f^{-1} \circ \eta(\mathbf{x}) &= \hat{\mathbf{p}} \\ &= (J^{\mathrm{T}}\Sigma^{-1}J)^{-1}J^{\mathrm{T}}\Sigma^{-1}(\mathbf{x}-\bar{\mathbf{x}}) + \bar{\mathbf{p}} \\ &= (J^{\mathrm{T}}\Sigma^{-1}J)^{-1}J^{\mathrm{T}}\Sigma^{-1}(\mathbf{x}-\bar{\mathbf{x}}) + f^{-1}(\bar{\mathbf{x}}) \\ &= f^{-1} \circ \eta(\bar{\mathbf{x}}) + (J^{\mathrm{T}}\Sigma^{-1}J)^{-1}J^{\mathrm{T}}\Sigma^{-1}(\mathbf{x}-\bar{\mathbf{x}})\,. \end{aligned} \tag{8}$$

This shows that $f^{-1} \circ \eta$ is affine and $(J^{\mathrm{T}}\Sigma^{-1}J)^{-1}J^{\mathrm{T}}\Sigma^{-1}$ is its linear part. Applying forward propagation of covariance, we see that the covariance matrix for $\hat{\mathbf{p}}$ is

$$\begin{aligned} {}_{\hat{\mathbf{p}}}\Sigma &= (J^{\mathrm{T}}\Sigma^{-1}J)^{-1}J^{\mathrm{T}}\Sigma^{-1}\Sigma\Sigma^{-\mathrm{T}}J(J^{\mathrm{T}}\Sigma^{-1}J)^{-\mathrm{T}} \\ &= J^{-1}\Sigma J^{-\mathrm{T}}J^{\mathrm{T}}\Sigma^{-1}\Sigma\Sigma^{-\mathrm{T}}J^{-1}\Sigma J^{-\mathrm{T}} \\ &= J^{-1}\Sigma J^{-\mathrm{T}} \\ &= (J^{\mathrm{T}}\Sigma^{-1}J)^{-1}\,, \end{aligned} \tag{9}$$

recalling that Σ is symmetric.

It is assumed that the cylindrical objects used for calibration are of known radius R. The parameter vector $\mathbf{p}$ in that case consists of $[x_c\ y_c]^{\mathrm{T}}$, i.e. circle centers. Measurement space is a vector of ranges that the laser range sensor produces for the corresponding cylinder. Since we assume independence of the individual LRS measurements, we can consider only one LRS measurement (r, φ). Mapping from parameter space to measurement space for this single reading is as follows

$$\begin{aligned} {}_C r &= \sqrt{x^2 + y^2} \\ x &= \frac{x_c + y_c \tan\varphi \pm \sqrt{D}}{1 + tan^2\varphi} \\ y &= x \tan\varphi \\ D &= (x_c + y_c \tan\varphi)^2 - (1 + tan^2\varphi)(x_c^2 + y_c^2 - R^2)\,. \end{aligned} \tag{10}$$

The Jacobian of this transformation at $[x_c\ y_c]^{\mathrm{T}}$ is given with

$$\begin{aligned} {}_C J &= \frac{\partial_C r}{\partial \mathbf{p}} \\ &= \begin{bmatrix} \frac{\partial_C r}{\partial x_c} & \frac{\partial_C r}{\partial y_c} \end{bmatrix} \\ &= \frac{1}{2}(x^2+y^2)^{-\frac{1}{2}} \begin{bmatrix} 2x\frac{\partial x}{\partial x_c} + 2y\frac{\partial y}{\partial x_c} & 2x\frac{\partial x}{\partial y_c} + 2y\frac{\partial y}{\partial y_c} \end{bmatrix} \\ &= \frac{1}{{}_C r} \begin{bmatrix} x\frac{\partial x}{\partial x_c} + y\frac{\partial x}{\partial x_c}\tan\varphi & x\frac{\partial x}{\partial y_c} + y\frac{\partial x}{\partial y_c}\tan\varphi \end{bmatrix} \\ \frac{\partial x}{\partial x_c} &= \frac{1 \pm D^{-\frac{1}{2}}(y_c \tan\varphi - x_c \tan^2\varphi)}{1 + \tan^2\varphi} \\ \frac{\partial x}{\partial y_c} &= \frac{\tan\varphi \pm D^{-\frac{1}{2}}(x_c \tan\varphi - y_c)}{1 + \tan^2\varphi}\,, \end{aligned} \tag{11}$$

where the ambiguous sign is determined by Eq. (10), i.e. out of two possible line and circle intersections, the one closer to the origin (LRS) is taken.

Finally, given all the measurements for a cylinder, estimated center uncertainty is given by

$${}_C\Sigma = \left(\sum_j {}_C J_j^{\mathrm{T}}\, {}_r\Sigma_j^{-1}\, {}_C J_j \right)^{-1}\,. \tag{12}$$

2.3 Estimating 2D Euclidean transform

2D Euclidean transform consists of rotation θ and translation $\mathbf{t}$. Having determined cylinder centers with both LR sensors ($\mathbf{x}_i$ and $\mathbf{x}'_i$), we can proceed to estimate Euclidean transform.

After translating cylinder centers for $\mathbf{t}_1$ and $\mathbf{t}_2$ to move them to their respective centroids, Kabsch algorithm (constrained orthogonal Procrustes problem) can be applied in order to determine rotation θ between those two point sets. Translation part of the transform is then

$$\mathbf{t} = Rot(\theta)\mathbf{t}_1 - \mathbf{t}_2\,, \tag{13}$$

where

$$Rot(\theta) = \begin{bmatrix} \cos\theta & -\sin\theta \\ \sin\theta & \cos\theta \end{bmatrix}\,. \tag{14}$$

Unfortunately, this is not an ML estimate given cylinder center uncertainties ${}_C\Sigma$. But it is a good starting point for solving the following minimization problem

$$\begin{aligned} \hat{\theta}_{mle}, \hat{\mathbf{t}}_{mle} = \underset{\theta,\mathbf{t},\bar{\mathbf{x}}_i}{\arg\min} \sum_i &(\mathbf{x}_i - \bar{\mathbf{x}}_i)^{\mathrm{T}}\, {}_C\Sigma_i^{-1}(\mathbf{x}_i - \bar{\mathbf{x}}_i) + \\ &(\mathbf{x}'_i - \bar{\mathbf{x}}'_i)^{\mathrm{T}}\, {}_{C'}\Sigma_i^{-1}(\mathbf{x}'_i - \bar{\mathbf{x}}'_i)\,, \end{aligned} \tag{15}$$

where $\bar{\mathbf{x}}'_i = Rot(\theta)\bar{\mathbf{x}}_i + \mathbf{t}$. Using Cholesky decomposition for matrices ${}_C\Sigma_i^{-1}$ and ${}_{C'}\Sigma_i^{-1}$ one can construct a criteria function that can be used with the readily available nonlinear least squares minimization algorithms.

2.4 Estimating 2D Euclidean transform uncertainty

In θ, $\mathbf{t}$ parametrization the transform is obviously nonlinear. It is usual to represent the transform in linear and over-parametrized form

$$H = \begin{bmatrix} Rot(\theta) & \mathbf{t} \\ \mathbf{0}^{\mathrm{T}} & 1 \end{bmatrix} \tag{16}$$

and represent points in homogeneous coordinates. In this case we have $\cos\theta$ and $\sin\theta$ instead of just θ.

In order to apply result for circle uncertainty in Eq. (9) we introduce mapping $g : \mathbb{R}^d \to \mathbb{R}^M$ from the space of essential parameters $\mathbb{R}^d$ to the parameter space $\mathbb{R}^M$. Now $f \circ g$ maps from essential parameter to measurement space. If the partial derivatives matrix of g is given by A, then the partial derivatives matrix of $f \circ g$ is JA. Given that, the covariance matrix of essential parameters is then given by

$${}_{\mathbf{h}^d}\Sigma = (A^{\mathrm{T}}J^{\mathrm{T}}\, {}_N\Sigma^{-1}JA)^{-1} \tag{17}$$

and the covariance matrix of parameters is given by

$${}_{\mathbf{h}^M}\Sigma = A(A^{\mathrm{T}}J^{\mathrm{T}}\, {}_N\Sigma^{-1}JA)^{-1}A^{\mathrm{T}}\,. \tag{18}$$

Assuming $\mathbf{h}^M = \begin{bmatrix}\cos\theta\ \sin\theta\ \mathbf{t}^{\mathrm{T}}\ \bar{\mathbf{x}}_1\ \ldots\ \bar{\mathbf{x}}_n\end{bmatrix}^{\mathrm{T}}$ and $\mathbf{h}^d = \begin{bmatrix}\theta\ \mathbf{t}^{\mathrm{T}}\ \bar{\mathbf{x}}_1\ \ldots\ \bar{\mathbf{x}}_n\end{bmatrix}^{\mathrm{T}}$ we get partial derivative matrices

$$A = \begin{bmatrix} -\sin\theta & 0_{2\times 2n} \\ \cos\theta & \\ 0_{2n\times 1} & I_{2n\times 2n} \end{bmatrix} \tag{19}$$

and

$$
{}_{\mathbf{h}^M}J = \frac{\partial \left[\bar{\mathbf{x}}_1^{\mathrm{T}} \ \dots \ \bar{\mathbf{x}}_n^{\mathrm{T}} \ \bar{\mathbf{x}}_1'^{\mathrm{T}} \ \dots \ \bar{\mathbf{x}}_n'^{\mathrm{T}}\right]^{\mathrm{T}}}{\partial \mathbf{h}^M}
$$

$$
= \left[\begin{array}{cccc:cccccc}
 & & & & & & & & & \\
 & & & & & & & & & \\
 & & & & & & & & & \\
 & 0_{2n\times 4} & & & & & I_{2n\times 2n} & & & \\
 & & & & & & & & & \\
 & & & & & & & & & \\
 & & & & & & & & & \\
\hdashline
\bar{\mathbf{x}}_{1,1} & -\bar{\mathbf{x}}_{1,2} & 1 & 0 & \cos\theta & -\sin\theta & & & & \\
\bar{\mathbf{x}}_{1,2} & \bar{\mathbf{x}}_{1,1} & 0 & 1 & \sin\theta & \cos\theta & & & 0 & \\
\vdots & & & & & & & \ddots & & \\
\bar{\mathbf{x}}_{n,1} & -\bar{\mathbf{x}}_{n,2} & 1 & 0 & & 0 & & & \cos\theta & -\sin\theta \\
\bar{\mathbf{x}}_{n,2} & \bar{\mathbf{x}}_{n,1} & 0 & 1 & & & & & \sin\theta & \cos\theta
\end{array}\right] . \tag{20}
$$

3. ALGORITHM EVALUATION ON REAL WORLD DATA

In this section we evaluate the proposed 2D Euclidean transform estimation algorithm on data obtained with two different SICK LR sensors. The algorithm is summarized in the pseudocode that follows.

1: **procedure** EstimateEuclideanTransform (LRS data, cylinder scan segments)
3: **for all** laser ∈ LRS **do**
4: **for all** segment ∈ cylinder segments **do**
5: $\hat{C} \leftarrow$ estimate cylinder center using Eq. (5)
6: ${}_C\Sigma \leftarrow$ estimate it's uncertainty using Eq. (12)
7: **end for**
8: **end for**
9: $\mathbf{t}_1 \leftarrow$ centroid of the LRS1 cylinder centers
10: $\mathbf{t}_2 \leftarrow$ centroid of the LRS2 cylinder centers
11: $Rot(\theta) \leftarrow$ by applying Kabsch algorithm on the resulting corresponding points
12: $\mathbf{t} \leftarrow Rot(\theta)\mathbf{t}_1 - \mathbf{t}_2$
13: $\hat{\theta}_{mle}, \hat{\mathbf{t}}_{mle} \leftarrow$ by minimizing Eq. (15) and using previous results for initialization
14: ${}_{\mathbf{h}^M}\Sigma \leftarrow$ by inserting Equations (19) and (20) into (18)
15: **end procedure**

The sensors used where LMS 200-30106 (indoor unit, mounted on Pioneer 3-DX) and LMS 291-S05 (outdoor unit, mounted on Pioneer 3-AT). The robots were placed in the opposite corners of a 7×6.5 m^2 room. Three fire extinguishers were used as calibration targets (cylindrical objects), placed in the center of the room, in the field of view of both LRS.

Circle estimate of the central cylinder in the FOV of the outdoor SICK unit, as shown in Fig. 2, was unexpected. It's center was estimated fairly closer to the LRS than truly is in order to have intersection points between the circle and the laser beams. Either our cylinder had larger radius than we thought, or there was something wrong with the sensor.

3.1 Modeling and measuring LRS bias

Technical specifications for LMS 291 state that the device has a bias of ±35 mm in it's millimeter mode (range in 1 to 20 m). The LMS 200 has somewhat smaller bias of ±15 mm, but it also has smaller range (from 1 to 8 m).

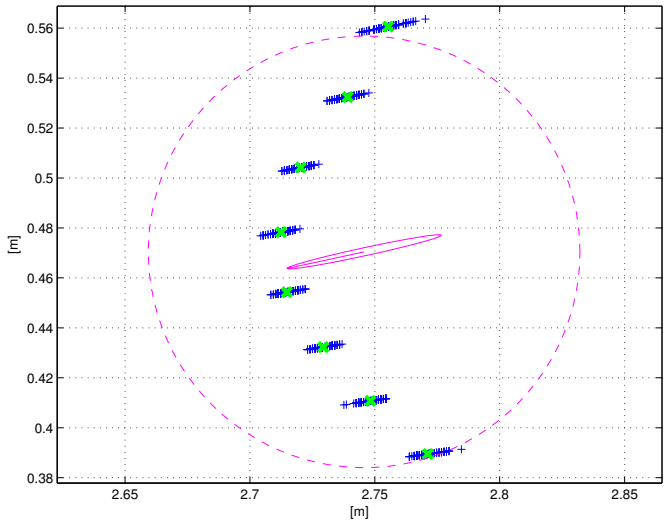

Fig. 2. Estimating circle from LMS 291 data. Blue crosses represent laser measurements (100 scans), green x is their mean. Estimated circle is drawn with dashed magenta line, and magenta ellipse is 10 times magnified 95% confidence region of circle center.

Given that, measured range is modeled as follows

$$
r_i = r_i^{\text{true}} + b + \delta r \,, \tag{21}
$$

where $\delta r \sim \mathcal{N}(0, \sigma_r^2)$. A convenient way to estimate bias is to measure a straight wall with as large FOV as possible. Wall (line) is given in Hess normal form with parameters (p, ϑ). The laser measurement (of that line) at angle φ_i is then

$$
{}_L r_i = \frac{p}{\cos(\varphi_i - \vartheta)} + b \,. \tag{22}
$$

Bias is found by minimizing the following criteria function

$$
\hat{b}_{mle} = \arg\min_{p,\vartheta,b} \sum_{i \in L} \left(r_i - {}_L r_i\right)^2 . \tag{23}
$$

You may notice that the line parameters are estimated as well. We found this to be easier than to place the laser so that line parameters are exactly known.

Results of bias estimation for SICK LMS 291 are shown in Fig. 3. Estimated bias was 24.5 mm. Following the same procedure, estimated bias for SICK LMS 200 was 11 mm.

3.2 Results after accounting for LRS bias

After accounting for LRS bias, circle estimate for central cylinder in LMS 291 FOV is shown in Fig. 4. Taking bias into account, we have managed to get a much better estimate for the cylinder center.

After running the algorithm, we got the following transform matrix

$$
H = \begin{bmatrix} Rot(-170.30°) & \begin{matrix} 4.75 \\ 1.26 \end{matrix} \\ \mathbf{0}^{\mathrm{T}} & 1 \end{bmatrix} . \tag{24}
$$

We also have got the full covariance matrix of the transform for use in point transfer covariance calculation. As an example, we got $\sigma_\theta = 0.033°$, $\sigma_{t_1} = 1.3$ mm and $\sigma_{t_2} = 1.61$ mm.

In order to test our estimate, we ran our algorithm 10 times on sequentially obtained data. Cylinders remained

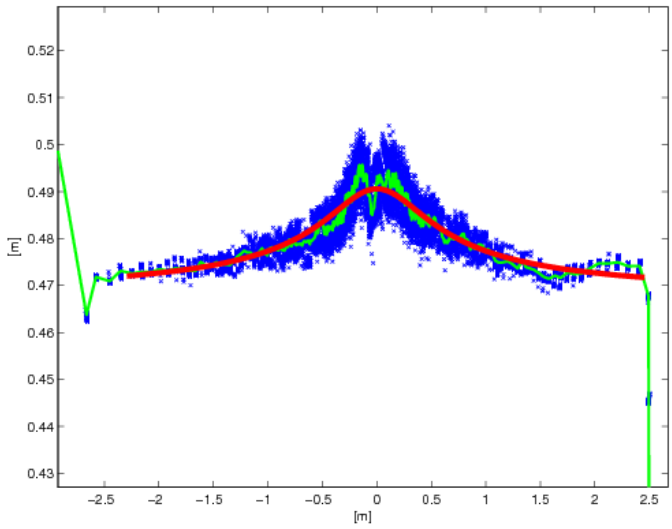

Fig. 3. Estimating LMS 291 bias. Blue x-es are laser measurements (100 scans). Green line connects their mean. Red line represents ideal readings of the estimated line with an LRS that has the estimated bias (24.5 mm in this case).

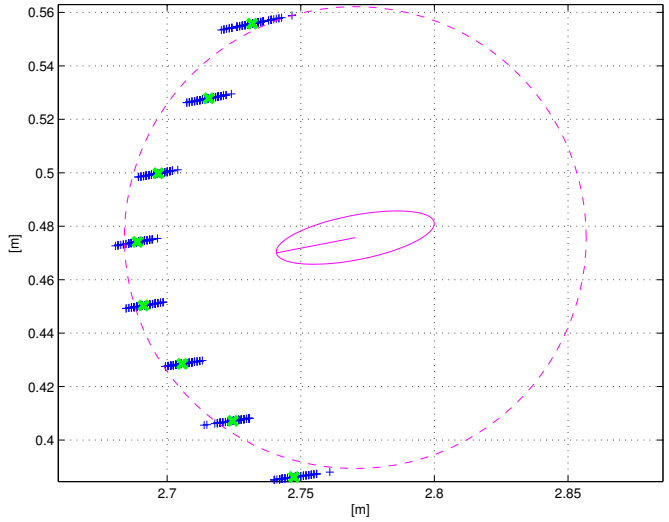

Fig. 4. Estimating circle from LMS 291 data. Bias is taken into account.

on the same location during the experiment. We obtained following standard deviations for those 10 estimates; $\sigma_\theta = 0.032°$, $\sigma_{t_1} = 3.21$ mm and $\sigma_{t_2} = 1.44$ mm. Except for σ_{t_1}, standard deviations do not deviate much from those reported by our algorithm. Some deviations were expected, because of linear approximations made in multiple steps of the algorithm.

4. CONCLUSION

In this paper we have presented an algorithm for 2D Euclidean transform estimation for laser range sensors. A calibration target is used, in form of cylindrical objects perpendicular to the sensing plane. Estimation of cylinder centers turned out to be very sensitive to laser bias. Therefore, in this paper we also proposed a method to estimate it.

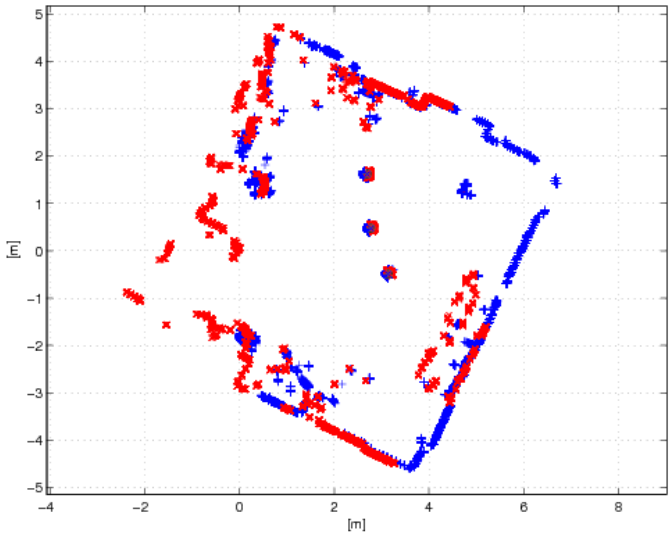

Fig. 5. Calibration results. Measurements from SICK LMS 200 (red x-es) are shown in the frame of SICK LMS 291 (blue crosses).

The results of this algorithm can be used to gather very precise ground truth for people tracking applications with LRS. In case of occlusions, one has obvious benefits from two or more different viewpoints. For people tracking, we could obtain exact positions for all possible individual leg configurations. This data would enable evaluating full CLEAR MOT metric (MOTA and MOTP).

REFERENCES

Bernardin, K. and Stiefelhagen, R. (2008). Evaluating multiple object tracking performance: the CLEAR MOT metrics. *Journal on Image and Video Processing*, 2008, 1.

Fod, A., Howard, A., and Mataric, M. (2002). Laser-based people tracking. In *Proc. of the IEEE International Conference on Robotics & Automation*. Citeseer.

Hartley, R. and Zisserman, A. (2004). *Multiple View Geometry in Computer Vision*, volume 16. Cambridge University Press. doi:10.1016/0010-4485(84)90252-5.

Kluge, B., Kohler, C., and Prassler, E. (2001). Fast and robust tracking of multiple moving objects with a laser range finder. In *Robotics and Automation, 2001. Proceedings 2001 ICRA. IEEE International Conference on*, volume 2, 1683–1688. IEEE.

Luber, M., Diego Tipaldi, G., and Arras, K.O. (2011). Place-dependent people tracking. *The International Journal of Robotics Research*, 30(3), 280–293. doi: 10.1177/0278364910393538.

Sasaki, T. and Hashimoto, H. (2011). Object Tracking for Calibration of Distributed Sensors in Intelligent Space. In H. Goszczynska (ed.), *Object Tracking*. InTech.

Schulz, D., Burgard, W., Fox, D., and Cremers, A.B. (2003). People Tracking with Mobile Robots Using Sample-Based Joint Probabilistic Data Association Filters. *The International Journal of Robotics Research*, 22(2), 99–116. doi:10.1177/0278364903022002002.

Topp, E.A. and Christensen, H.I. (2005). Tracking for following and passing persons. In *Intelligent Robots and Systems, 2005.(IROS 2005). 2005 IEEE/RSJ International Conference on*, 2321–2327. IEEE.